PHILOSOPHICAL TRANSACTIONS OF THE ROYAL SOCIETY A

Phil. Trans. R. Soc. A (2012) **370**, 4927–4943
doi:10.1098/rsta.2012.0198

Review

Cationic-vacancy-induced room-temperature ferromagnetism in transparent, conducting anatase $Ti_{1-x}Ta_xO_2$ ($x \sim 0.05$) thin films

By A. Rusydi[1,2,3,*,†], S. Dhar[1,4,*,†], A. Roy Barman[1,2,†], Ariando[1,2], D.-C. Qi[1,2], M. Motapothula[1,2], J. B. Yi[5], I. Santoso[1,2], Y. P. Feng[1,2], K. Yang[2,6], Y. Dai[6], N. L. Yakovlev[7], J. Ding[1,5], A. T. S. Wee[1,2], G. Neuber[8,9], M. B. H. Breese[1,2,3], M. Ruebhausen[1,8,9], H. Hilgenkamp[1,10] and T. Venkatesan[1,2,4,*]

[1]*NUSNNI-NanoCore, National University of Singapore, Singapore 117411, Republic of Singapore*
[2]*Department of Physics, National University of Singapore, Singapore 117542, Republic of Singapore*
[3]*Singapore Synchrotron Light Source, National University of Singapore, Singapore 117603, Republic of Singapore*
[4]*Department of Electrical and Computer Engineering, and*
[5]*Department of Materials Science and Engineering, National University of Singapore, Singapore 117576, Republic of Singapore*
[6]*School of Physics, State Key Laboratory of Crystal Materials, Shandong University, Jinan 250100, People's Republic of China*
[7]*Institute of Materials Research and Engineering, A*STAR, Singapore 117602, Republic of Singapore*
[8]*Institut für Angewandte Physik, Universität Hamburg, 20355 Hamburg, Germany*
[9]*Center for Free Electron Laser Science (CFEL), 22607 Hamburg, Germany*
[10]*Faculty of Science and Technology, MESA+ Institute for Nanotechnology, University of Twente, PO Box 217, 7500 AE Enschede, The Netherlands*

We report room-temperature ferromagnetism (FM) in highly conducting, transparent anatase $Ti_{1-x}Ta_xO_2$ ($x \sim 0.05$) thin films grown by pulsed laser deposition on $LaAlO_3$ substrates. Rutherford backscattering spectrometry (RBS), X-ray diffraction, proton-induced X-ray emission, X-ray absorption spectroscopy (XAS) and time-of-flight secondary-ion mass spectrometry indicated negligible magnetic contaminants in the films. The presence of FM with concomitant large carrier densities was determined by a combination of superconducting quantum interference device magnetometry,

*Authors for correspondence (phyandri@nus.edu.sg; eleds@nus.edu.sg; venky@nus.edu.sg).

†These authors contributed equally to this work.

One contribution of 10 to a Discussion Meeting Issue 'The new science of oxide interfaces'.

electrical transport measurements, soft X-ray magnetic circular dichroism (SXMCD), XAS and optical magnetic circular dichroism, and was supported by first-principles calculations. SXMCD and XAS measurements revealed a 90 per cent contribution to FM from the Ti ions, and a 10 per cent contribution from the O ions. RBS/channelling measurements show complete Ta substitution in the Ti sites, though carrier activation was only 50 per cent at 5 per cent Ta concentration, implying compensation by cationic defects. The role of the Ti vacancy (V_{Ti}) and Ti^{3+} was studied via XAS and X-ray photoemission spectroscopy, respectively. It was found that, in films with strong FM, the V_{Ti} signal was strong while the Ti^{3+} signal was absent. We propose (in the absence of any obvious exchange mechanisms) that the localized magnetic moments, V_{Ti} sites, are ferromagnetically ordered by itinerant carriers. Cationic-defect-induced magnetism is an alternative route to FM in wide-band-gap semiconducting oxides without any magnetic elements.

Keywords: dilute magnetic semiconductor oxides

1. Introduction

Because of the many potential applications in spintronics, magneto-optical and opto-electronic devices, extensive efforts are being made to introduce room-temperature (RT) ferromagnetism (FM) into various wide-band-gap semiconducting oxides and III–V and II–VI based semiconducting systems [1–15]. Considerable success has been achieved in the production of dilute magnetic semiconductors (DMS) by introducing a magnetic impurity into a non-magnetic host material. The most reproducible carrier-induced FM in semiconductors is based on Mn doping of GaAs, but its Curie temperature, T_C, is limited to about 173 K [3,7]. Among the oxides, the most notable compounds exhibiting DMS behaviour above RT are based on TiO_2 and ZnO [8–15]. Despite these developments, magnetic-impurity-based DMS oxides are the subject of intense debate as a result of the many inconsistent results related to secondary phase formation, unknown impurities or substitutionality, solubility, clustering and/or segregation of the magnetic impurities in the host oxide matrix [16–18]. More recently, there have been reports of FM in ZnO and other oxides (attributed to anionic vacancies) by doping with non-magnetic ions, but besides evidence from superconducting quantum interference device (SQUID) data [13–15], a necessary but not sufficient criterion [17,18], there has been no reliable element-specific evidence for FM in these cases, with the exception of recent publications [19,20]. To establish true FM in the DMS oxides and to differentiate from impurity artefacts, various magnetic measurements—ranging from extremely sensitive SQUID and optical magnetic circular dichroism (OMCD) measurements, which directly probe the spin-polarized bands, to element-specific soft X-ray magnetic circular dichroism (SXMCD) measurements—are required.

The idea of cationic-vacancy-induced FM (with concomitant half-metallicity) in wide-band-gap semiconducting oxides was proposed on theoretical grounds by Elfimov *et al.* [21], and later Osorio-Guillén *et al.* [22] pointed out that either hole or electron doping facilitates the formation of cationic vacancies. It was predicted that wide-band-gap CaO could become a half-metallic ferromagnet with about 3–5% cationic (Ca) vacancies. However, the realization of high-quality films of CaO

has not yet been achieved as a result of the hygroscopic nature of CaO, which leads to rather unstable films. The first experimental observation of a local magnetic moment arising from a cationic vacancy was reported by Zhang *et al.* [23], who observed signatures of the Kondo effect below 100 K in 5 per cent Nb-doped anatase TiO_2 thin films grown under 10^{-4} Torr oxygen partial pressure by pulsed laser deposition (PLD). Using X-ray absorption spectroscopy (XAS) and X-ray photoemission spectroscopy (XPS), supported by first-principles calculations, they showed that the appearance of Kondo scattering was due to the presence of localized magnetic moments associated with cationic (Ti) vacancies produced as a result of Nb incorporation. However, no FM was observed, which is presumably due to the low concentration of Ti vacancies (V_{Ti}) and free carriers [8]. On the other hand, from structural considerations, Osorio-Guillén *et al.* [22] suggested that it would be difficult to create films having cationic vacancies larger than 3 per cent. In this paper, we report the production of V_{Ti} and room-temperature FM over a narrow processing range in (001) anatase $Ti_{1-x}Ta_xO_2$ ($x \sim 0.05$) thin films grown on (001) $LaAlO_3$ substrates. We show that Ta^{5+} gives rise to free charge carriers and cationic defects, i.e. V_{Ti} and Ti^{3+} are created as compensating centres depending on the processing conditions. From XMCD, the relative contributions to FM from cationic versus anionic defects are in the ratio of 9 to 1. The appearance of FM is proposed to be due to the formation of V_{Ti} (with delocalized V_{Ti} magnetic orbitals) coupled by the itinerant electron-carrier-mediated Ruderman–Kittel–Kasuya–Yosida (RKKY) exchange interaction.

2. Experimental method

Very high-purity (99.999%) Ta_2O_5 and TiO_2 powders were ground for several hours before sintering in a furnace at 1000°C in air for 20 h. Next, target pellets were made and sintered at 1100°C in air for 24 h. Anatase $Ti_{1-x}Ta_xO_2$ epitaxial thin films (with $x = 0$ and 0.1) of thicknesses between 50 and 500 nm were deposited on high-quality (001) $LaAlO_3$ substrates by PLD, using a 248 nm Lambda Physik (Germany) excimer laser with an energy density of 1.8 J cm^{-2} and a repetition rate of 2–10 Hz. Depositions were performed for 0.5–1 h in a stable oxygen partial pressure of 1×10^{-5} Torr while the substrate temperature was maintained at various temperatures in the range of 500–800°C. The chemical and structural properties of the samples were studied by XPS, electrical transport measurements, SQUID, XAS, SXMCD, OMCD, Rutherford backscattering spectrometry (RBS)/channelling, X-ray diffraction (XRD) and time-of-flight secondary-ion mass spectrometry (TOF-SIMS).

3. Results and discussion

In this study, we found that the preferred temperature of growth for a highly crystalline pure TiO_2 film was about 750°C, and we observed a catalytic effect of Ta on TiO_2, which reduced the crystallization temperature with increasing Ta concentrations. While FM was demonstrated on many samples, we present here four types of films to illustrate the role of V_{Ti} and Ti^{3+} as the origin of FM in this system: pure TiO_2 films grown at 600°C and 750°C, and $Ti_{1-x}Ta_xO_2$ ($x \sim 0.05$) films grown at 600°C and 750°C.

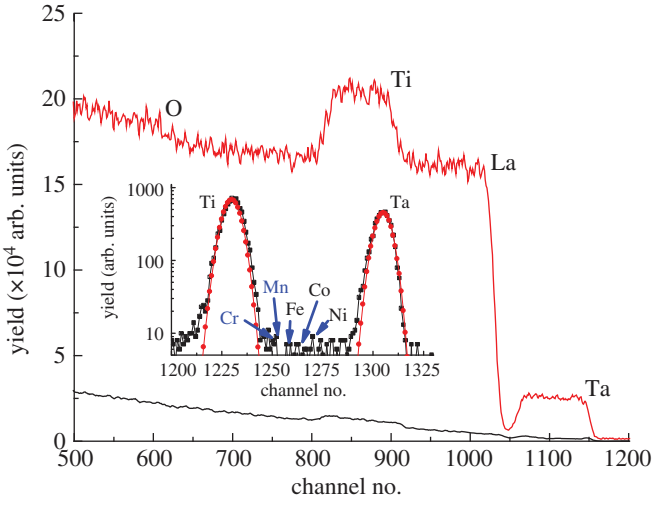

Figure 1. RBS random (upper red line) and channelling (lower black line) spectra of $Ti_{1-x}Ta_xO_2$ ($x \sim 0.05$) films grown on $LaAlO_3$ substrate. Inset: a random RBS spectrum of an identical sample grown on Si substrate. (Online version in colour.)

(*a*) *Structural, chemical, electrical and optical properties*

The formation of *c*-axis-oriented anatase TiO_2 was confirmed in all $Ti_{1-x}Ta_xO_2$ films by XRD analysis, and no other phases were observed within its detection limit. Using ultraviolet–visible spectroscopy, the optical band gaps of the pure and doped samples were found to be 3.32 and 3.4 eV, respectively. The actual Ta concentrations in the films were found to be about $5.5 \pm 0.3\%$ by RBS (figure 1), and the ion channelling spectra show that most (99%) of the Ta was substitutional and probably in the Ti sites.

The contents of magnetic trace elements were measured using TOF-SIMS with 25 kV Bi analysis ions and 3 kV Ar sputtering ions. Because the main aim of this measurement was to determine the content of magnetic impurity elements, a reference target containing 1 at.% each of Cr, Mn, Fe, Co and Ni and 95 per cent of Ti, as measured by the weight of the respective oxides, was prepared. A film from this calibration target was made under the same conditions as used to produce the Ta-substituted TiO_2 ferromagnetic films. The intensities of the various elemental peaks in the SIMS mass spectra were integrated and normalized to that of ^{46}Ti. The relative sensitivity factors of these elements were determined from their intensities in the reference sample, and then the contents of all elements were estimated (figure 2). Unintended magnetic impurities (Fe, Ni, Mn, Co, Cr) were found to be substantially below 0.01 per cent (about three orders of magnitude less than the Ta concentration and roughly five orders of magnitude lower than the Ti concentration) in all samples by RBS (inset of figure 1), TOF-SIMS and wide-scan XAS (not shown here). Therefore, the polarizing effect (a possibility) of magnetic impurities on Ti ions can be clearly ruled out.

The XPS data in figure 3 show peaks at 459.1 eV (Ti $2p_{3/2}$) and 464.8 eV (Ti $2p_{3/2}$) that originate from Ti^{4+}, while the peaks at 457.3 and 462.4 eV are from Ti^{3+}, confirming that Ti is predominantly in the 4+ state for both

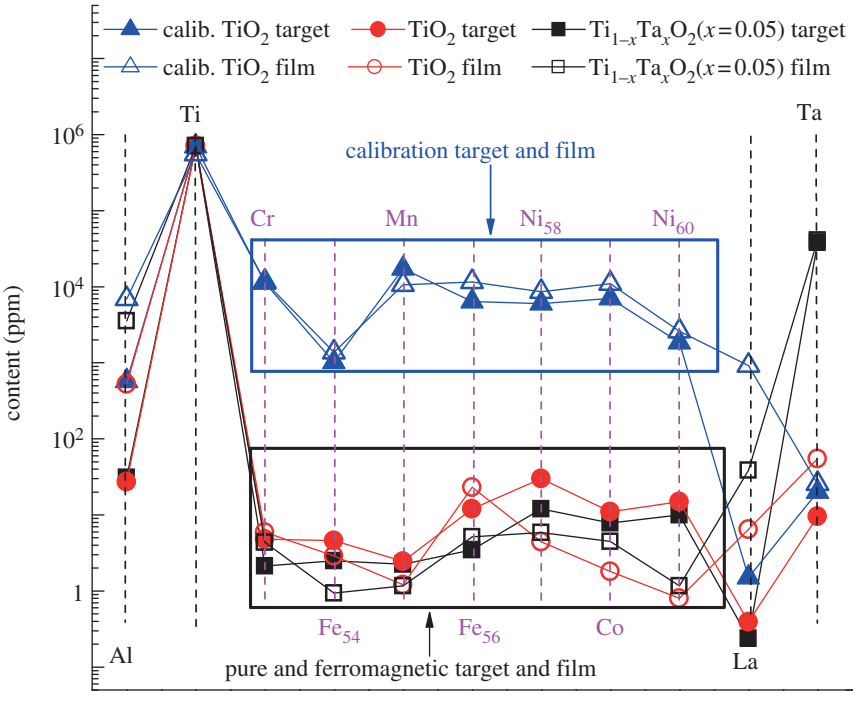

Figure 2. TOF-SIMS spectra from pure TiO_2 and $Ti_{1-x}Ta_xO_2$ ($x \sim 0.05$) targets and films grown on Si and $LaAlO_3$ substrates, along with spectra obtained from corresponding magnetic calibration samples. (Online version in colour.)

pure TiO_2 and $Ti_{1-x}Ta_xO_2$ ($x \sim 0.05$) samples. Our detailed analysis suggested that the Ti^{3+}/Ti^{4+} ratios for pure TiO_2 (figure 3*a*) and $Ti_{1-x}Ta_xO_2$ ($x \sim 0.05$) (figure 3*b*) films grown at 600°C were approximately 0.65 per cent and 0.59 per cent, respectively, while it was 8.45 per cent for the $Ti_{1-x}Ta_xO_2$ ($x \sim 0.05$) films grown at 750°C (figure 3*c*) [24]. The Ta was found to be in the 5+ state in all the films [25]. It may be noted that the Ti^{4+} state is non-magnetic while the Ti^{3+} state is magnetic.

The electron carrier concentration of the n-type pure anatase TiO_2 sample was of the order of 10^{17} to $10^{19}\,cm^{-3}$. After 5 at.% Ta incorporation, the n-type $Ti_{1-x}Ta_xO_2$ ($x \sim 0.05$) films became highly conductive. The RT electron carrier density and Hall mobility of $Ti_{1-x}Ta_xO_2$ ($x \sim 0.05$) films grown at 600°C were found to be about $7.66 \times 10^{20}\,cm^{-3}$ and $13.7\,cm^2\,V^{-1}\,s^{-1}$, respectively, while for the 750°C films they were $4.90 \times 10^{20}\,cm^{-3}$ and $11.9\,cm^2\,V^{-1}\,s^{-1}$, respectively. The full carrier activation was incomplete for all the Ta concentrations, implying carrier compensation that peaked at about 5–6% Ta concentration [26].

(*b*) *Magnetic properties*

To study the ferromagnetic properties, SQUID measurements were performed on the pure TiO_2 and $Ti_{1-x}Ta_xO_2$ ($x \sim 0.05$) thin films in a number of samples grown under different Ta concentrations, temperatures and oxygen partial pressures. In a study involving more than 60 samples, the magnetization tended

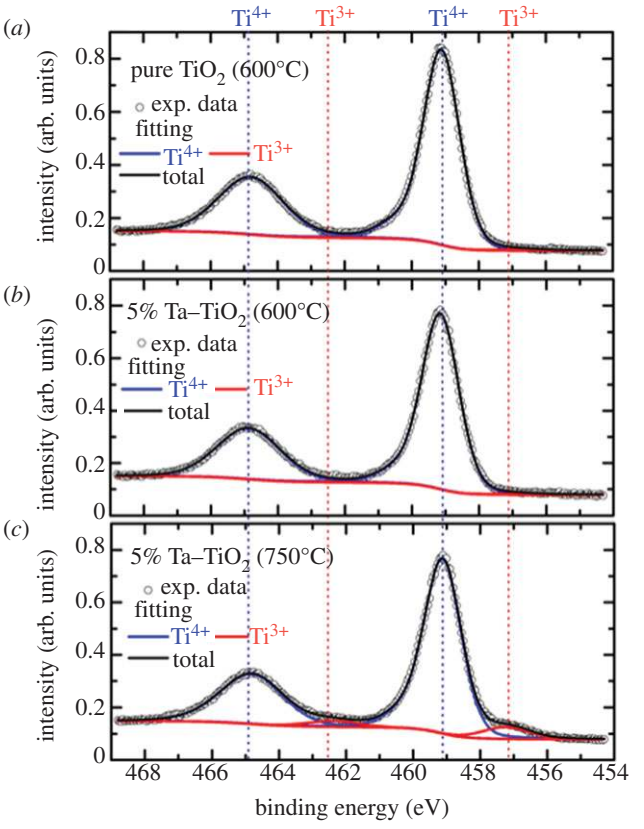

Figure 3. The XPS analysis of $Ti_{1-x}Ta_xO_2$ ($x \sim 0.05$) films at the Ti 2p core levels: (*a*) pure TiO_2 film grown at 600°C; and $Ti_{1-x}Ta_xO_2$ ($x \sim 0.05$) films grown at (*b*) 600°C and (*c*) 750°C. (Online version in colour.)

to peak at a Ta concentration of about 5–6%, a deposition temperature of about 600°C (repeated for about 20 samples) and an oxygen pressure of about 10^{-5} Torr.

A large number of samples prepared at optimum conditions showed FM, with saturation magnetization ranging from 1 to 4 emu g^{-1}, and coercive fields ranging from 70 to 90 Oe. Efforts are being made to narrow down the scatter in the saturation magnetization value. In order to obtain a better signal-to-noise ratio in other measurements, we used samples that showed saturation magnetization values close to 4 emu g^{-1}. A magnetization curve for a $Ti_{1-x}Ta_xO_2$ ($x \sim 0.05$) film grown at 600°C along with the one obtained from a pure TiO_2 film (non-magnetic) is shown in figure 4. In $Ti_{1-x}Ta_xO_2$ ($x \sim 0.05$) films grown at 600°C, the magnetization of 4 emu g^{-1} implies 1.1 μ_B/Ta using 5.5 per cent Ta ions (obtained from the RBS analysis). However, later analysis will reveal that Ta is not directly responsible for the FM; rather, V_{Ti} induced by the Ta are responsible. In the same figure, the magnetization for a higher-crystallinity $Ti_{1-x}Ta_xO_2$ ($x \sim 0.05$) film grown at 750°C is also shown, with magnetization values less by a factor of approximately 20, suggesting the possible role of defects in the FM. The

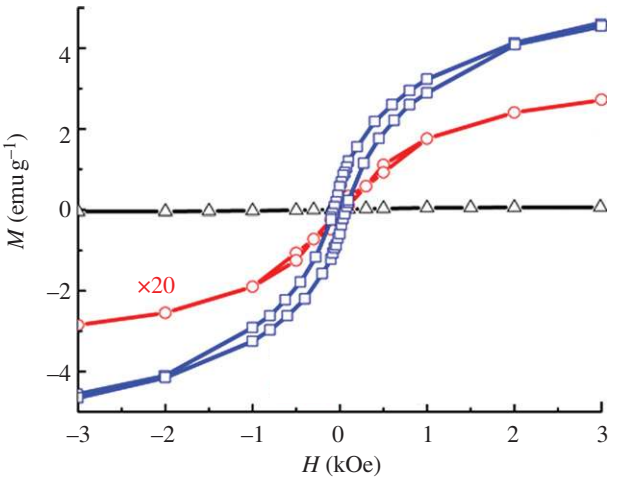

Figure 4. Magnetic hysteresis loops for pure TiO_2 at 600°C (triangles) and for $Ti_{1-x}Ta_xO_2$ ($x \sim 0.05$) thin films grown at 600°C (squares) and 750°C (circles) in an oxygen partial pressure of 1×10^{-5} Torr. (Online version in colour.)

$LaAlO_3$ substrate treated under similar process conditions (oxygen pressure and temperature but no film deposition) showed only diamagnetic behaviour. The Curie temperature T_C of the sample was well above 100°C, above which reliable measurements are hard due to gradual modification of the material.

Although the SQUID data clearly show the presence of room temperature FM in the $Ti_{1-x}Ta_xO_2$ ($x \sim 0.05$) films (prepared at 600°C), they do not provide microscopic insight into the origin of the ferromagnetic ordering. Thus, SXMCD measurements were performed in total yield mode as a function of photon energy, using elliptically polarized light with a degree of circular polarization $p = 90$ and an energy resolution of 0.25 eV at the SINS beam line of the Singapore Synchrotron Light Source [27] because this technique is not only element-specific but also capable of estimating both the spin and orbital magnetic moments and their anisotropies [28–30]. To measure the in-plane magnetic moments, the light was incident at a grazing angle of 20° from the sample surface, with its propagation direction along the sample in-plane magnetization direction. An external saturation magnetic field of up to 2000 Oe was applied to magnetize the sample along the in-plane direction. The SXMCD is the difference between two XAS spectra in the soft energy range taken with different light polarizations or different magnetic field directions. To avoid any ambiguity, both methods were applied. In the first method, the XAS data were taken with two opposite circular polarizations relative to a fixed sample magnetization direction (this was achieved by turning on a 0.2 T field for a short duration). The absorption coefficients, μ^+ and μ^-, which are directly proportional to XAS, have a photon helicity (spin) direction parallel (μ^+) and anti-parallel (μ^-) to the sample magnetization and magnetic field (M, H) direction, respectively [27,28]. Therefore, the SXMCD is equal to $(\mu^- - \mu^+)$. In the second method, the XAS data were taken with two opposite sample magnetization directions while fixing one of the directions of the circular polarized light. It is important to note that these two methods yield very

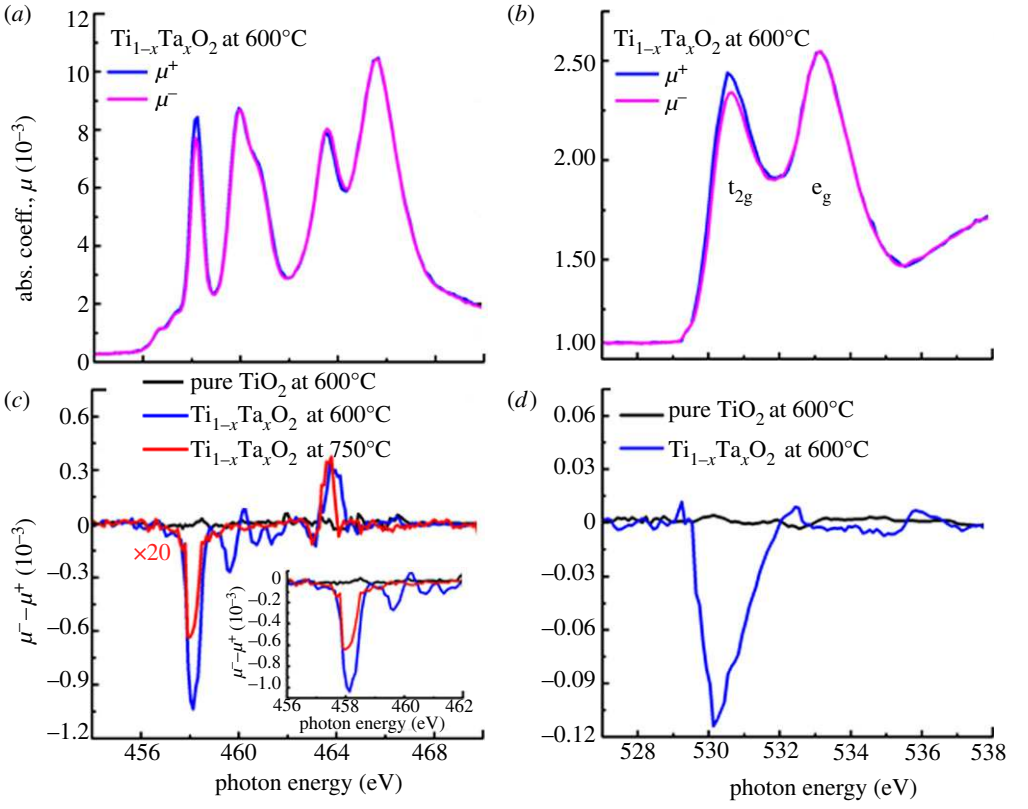

Figure 5. The absorption coefficient μ at (a) Ti $L_{2,3}$ edges and (b) O K edge of pure TiO_2 and $Ti_{1-x}Ta_xO_2$ ($x \sim 0.05$) films grown at 600°C and 750°C, where μ^+ and μ^- are parallel and anti-parallel alignments between the photon helicity and the sample magnetization direction. The corresponding SXMCD spectra for the (c) Ti $L_{2,3}$ edges and (d) the O K edge. (Online version in colour.)

similar results, indicating that the SXMCD results directly reflect the intrinsic properties of the films. The detection mode for both the SXMCD and XAS measurements was total electron yield (probing less than 20 nm) and fluorescence yield (probing less than 200 nm). Because the signal-to-noise ratio of the electron yield was superior, we only show here the total electron yield data.

The SXMCD data of $Ti_{1-x}Ta_xO_2$ ($x \sim 0.05$) films grown at 600°C and 750°C taken without any external magnetic field are shown in figure 5. In order to compare the SXMCD results at various edges, the SXMCD data were normalized to an absolute scale by fitting to the Henke tables [31] far below and above the edges, and then the absorption coefficients μ^+ (parallel) and μ^- (anti-parallel) were calculated. The advantage of this procedure is that it can be applied to most resonant edges in the soft X-ray range and thus allows us to compare the absorption coefficients at various edges [32–35], i.e. the Ti $L_{2,3}$ edges ($2p \rightarrow 3d$ transitions) and the O K edge (O $1s \rightarrow 2p$ transition) for this study. The μ^+ and μ^- at the Ti $L_{2,3}$ edge consist of two sets of peaks separated by 5–6 eV due to core hole spin–orbit coupling [36,37] of Ti $2p_j$ with $j = 1/2$ or $3/2$. Moreover, owing

Table 1. SXMCD peaks and corresponding transitions at the Ti L and O K edges.

peak position of SXMCD signal (eV)	elemental edge	transition
458.2	Ti	$2p_{3/2} \rightarrow 3d(t_{2g})$
460.0	Ti	$2p_{3/2} \rightarrow 3d(e_g)$
463.5	Ti	$2p_{1/2} \rightarrow 3d(t_{2g})$
465.5	Ti	$2p_{1/2} \rightarrow 3d(e_g)$
530.6	O	$1s \rightarrow$ Ti $3d(t_{2g})$
533.2	O	$1s \rightarrow$ Ti $3d(e_g)$

to ligand-field splitting, the 3d bands can be identified as t_{2g} and e_g symmetry bands. As a result, the Ti $2p \rightarrow 3d$ transitions consist of four dominant structures, and all the relevant transitions are shown in table 1. It may be noted that the Ta $L_{3,2}$ edges are expected to occur at around 9881 and 11136 eV, which are outside of the soft X-ray range [31].

The μ^+ and μ^- at the Ti $L_{2,3}$ and O K edges of the $Ti_{1-x}Ta_xO_2$ ($x \sim 0.05$) sample are shown in figure 5*a*,*b*, respectively. The SXMCD spectra in figures 5*c* and 4*d* correspond to the remnant magnetization, and are the most direct evidence for the intrinsic FM [17]. The SXMCD signals are surprisingly robust despite the fact that there was no applied magnetic field during the measurement. The observation of remnant SXMCD signals rules out the possibility of superparamagnetism [29–31]. In contrast, the pure TiO_2 film did not show any SXMCD signal at both resonant Ti $L_{2,3}$ and O K edges. Further, higher-crystallinity samples grown at 750°C showed an SXMCD (figure 5*c*) signal approximately 20 times smaller, consistent with the SQUID measurement.

The fact that both the Ti L and O K edge showed SXMCD signals predominantly in the t_{2g} state indicates a strong p–d hybridization and suggests that the t_{2g}-derived state plays a dominant role in the observed FM in this system. By applying the X-ray MCD sum rule [28,29], we obtained that the contribution to the orbital magnetic moment of Ti was nine times stronger than that of O and the spin alignments at Ti and O were parallel. These data confirm unambiguously that the origin of the FM is related to the Ti sites.

We further investigated the nature of this magnetism via OMCD, which is a photon-in and photon-out measurement, with an extended Sentech SE850 ellipsometer at the University of Hamburg, Germany. It covered an energy range from 0.5 to 5.5 eV, and was equipped with an ultra-high-vacuum cryostat. For spectral generalized magneto-optical ellipsometry (SGME), additional mounted Helmholtz coils enable the application of a fast-switching external magnetic field of 4500 Oe in transverse magneto-optical Kerr effect (TMOKE) geometry [38]. As the penetration depth was above 200 nm in this energy range, the whole film was scanned optically.

Figure 6*a* displays the differential intensity change $\delta I/I$ as a function of photon energy from 2 to 5 eV at various magnetic fields for the $Ti_{1-x}Ta_xO_2$ ($x \sim 0.05$) film grown at 600°C. The position of the measured optical band gap of 3.42 eV is shown by the vertical dashed line. It is seen from the figure that the transitions around 3.5 and 4.5 eV are strongly influenced by the applied magnetic field. The change

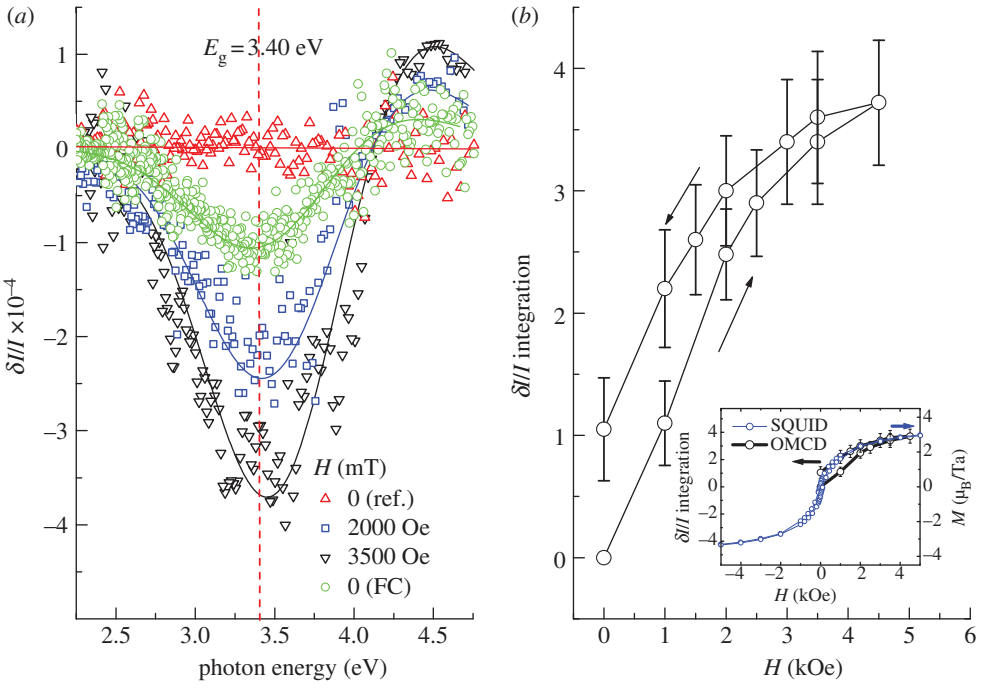

Figure 6. (*a*) OMCD signals obtained from a $Ti_{1-x}Ta_xO_2$ ($x \sim 0.05$) film grown at 600°C showing the dichroism and spin-polarized magnetization near the optical band gap. The vertical dashed line represents the position of the optical band gap. (*b*) Magnetic hysteresis loop from the OMCD measurement showing ferromagnetic behaviour. Inset: this loop is overlapped with the 40 K SQUID data. (Online version in colour.)

in sign of $\delta I/I$ at 4.5 eV is due to the optical transitions from non-spin-polarized occupied states to two possible unoccupied states: the majority-spin states at the Fermi energy E_F and the minority-spin states roughly 1 eV above E_F. The spin-splitting energy between the up-spin (majority spin) and the down-spin (minority spin) and the spin polarization of carriers at the optical band gap was about 1 eV, which is similar to those found in colossal magneto-resistive manganites [39], suggesting a strong electron localization effect (in energy or k space) in this present system. Assuming that the bands close to the Fermi energy (E_F) have a low density of states, the width of the transition at 3.5 eV of about 0.7 eV corresponds to the width of the majority-spin band. This strongly suggests that the occupied states correspond to O 2p states, whereas the majority- and minority-spin unoccupied states correspond to Ti 3d states. We next plot (figure 6*b*) the integrated absolute value of the OMCD signal between 2.2 and 4.1 eV and between 4.2 and 4.75 eV as a function of the applied magnetic field going from 0 to 4500 Oe and back. The hysteresis loop obtained from the SQUID measurement overlaps quite well (inset of figure 6*b*) with the OMCD data. It is worth noting that the OMCD signal is significant and indicates that we have an intrinsic FM as it is also connected to the optical band gap, i.e. the electronic density of states of the intrinsic band structure. These results further support that the FM seen in all the magnetization measurements came from the same source.

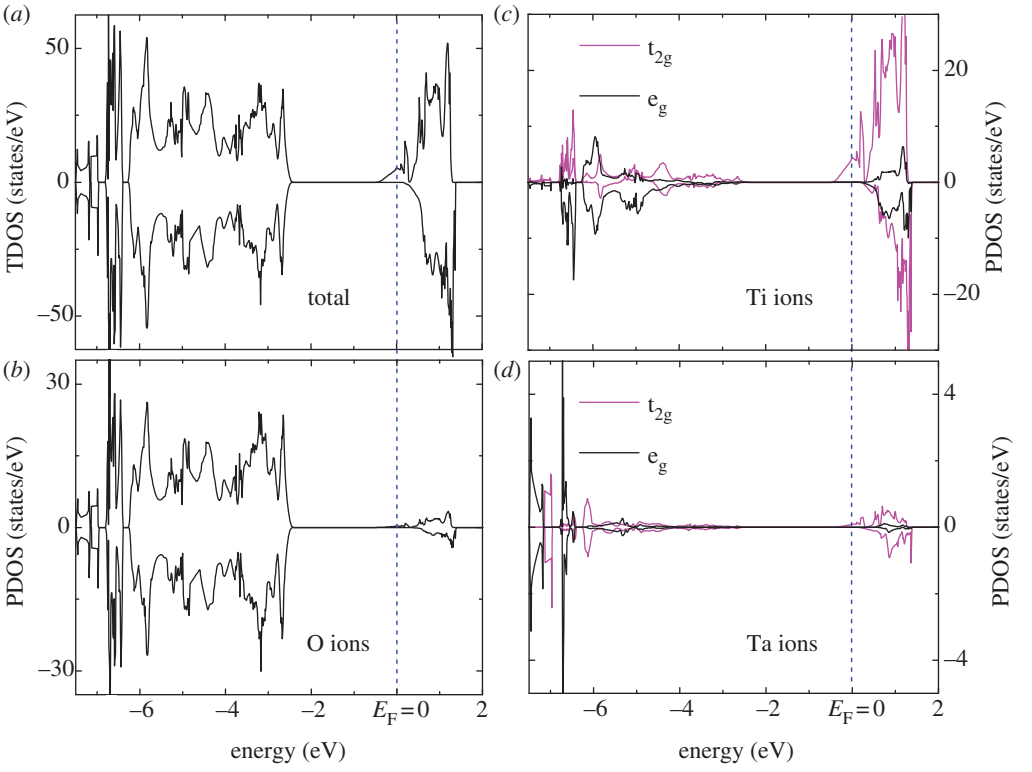

Figure 7. Calculated density of states of Ta incorporated anatase TiO_2 system: (*a*) total DOS, (*b*) partial DOS for O 2p states, (*c*) t_{2g} and e_g of Ti 3d and (*d*) t_{2g} and e_g of Ta 5d. (Online version in colour.)

(*c*) *Theoretical calculation*

To get further insight, first-principles calculations within a spin-polarized generalized-gradient approximation plus the on-site U parameter (GGA + U) were performed. A 48-atom super-cell, modelled by $2 \times 2 \times 1$ repetition of the 12-atom conventional unit cell of anatase TiO_2, which is proportional to 6.25 per cent Ta doping, was employed to study the electronic structure of $Ti_{1-x}Ta_xO_2$ films. Owing to computational difficulties, the 6.25 per cent Ta dopant was used instead of the actual 5.5 per cent Ta, but this does not change the main conclusions. The effective on-site U parameter ($U_{\text{eff}} = U - J$) of 5.8 eV and a scissor operator were used to make the calculated band gap comparable with the experimental value. The calculated electronic structures are shown in figure 7*a–d*. Interestingly, the magnetic moment mainly resides in Ti 3d(t_{2g}) bands that are hybridized with O 2p bands, which is consistent with the SXMCD results. Our calculations also indicated that an isolated V_{Ti} produced a high-spin-polarization electronic state, which was mainly contributed by the O 2p orbital of the first-nearest O atoms around the V_{Ti}. Furthermore, the V_{Ti}–V_{Ti} interaction resulted in a stable ferromagnetic ground state. It is important to mention that the spin-polarized density induced by the V_{Ti} extends

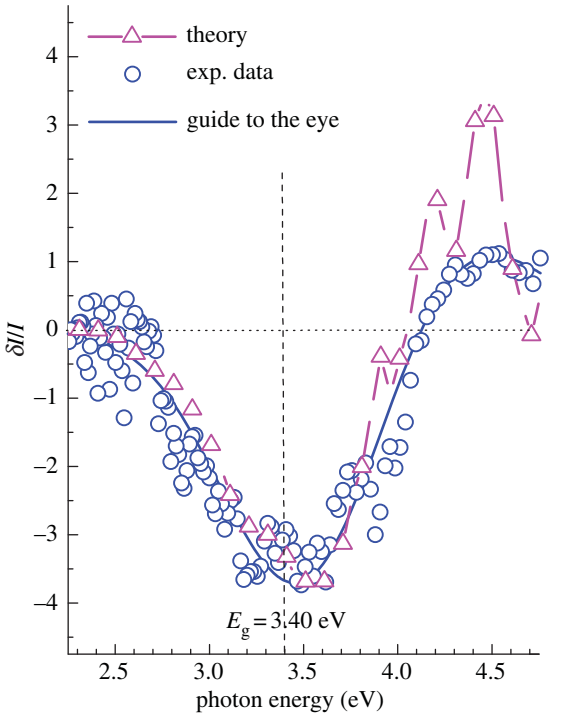

Figure 8. Comparison between experimental and calculated OMCD data. The blue line through the OMCD experimental data points is a guide to the eye only. (Online version in colour.)

very far to the third- and even to the fifth-nearest O atoms. As a result, the spin-polarized V_{Ti} orbitals were delocalized. When the magnetic orbitals of two V_{Ti} overlap through the common spin-polarized, third- and fifth-nearest O atoms, the overlapping spin density is non-zero, thereby leading to a long-range ferromagnetic alignment between the magnetic orbitals of two V_{Ti} [40]. In this process, free electron carriers are expected to facilitate the spin exchange coupling interaction between them. Our calculations also indicate that the Ti^{3+}–Ti^{3+} interaction favours antiferromagnetism. This also fully supports our experimental observations in which the sample with high Ti^{3+}, i.e. Ta–TiO_2 grown at 750°C Ta, has weak FM. Furthermore, the splitting energy between up-spin (majority-spin) and down-spin (minority-spin) Ti 3d states is about 1.1 eV. This value is also consistent with the OMCD measurements of $Ti_{1-x}Ta_xO_2$ ($x \sim 0.05$) film grown at 600°C shown in figure 6*a*, with a measured spin-splitting energy of about 1 eV. The calculated OMCD based on the density of states (DOS) is compared with the experimental results for the $Ti_{1-x}Ta_xO_2$ ($x \sim 0.05$) film grown at 600°C in figure 8. Owing to the quantum mechanical selection rules for optical absorption, the spin-polarized majority and minority states are directly connected with the appearance of a magneto-optical response. In the energy range of 2–5 eV, the optical transitions are dominated by charge transfer excitations between O 2p and Ti 3d. The calculations considered the inter-site transition from the spin-up (spin-down) occupied O 2p states to

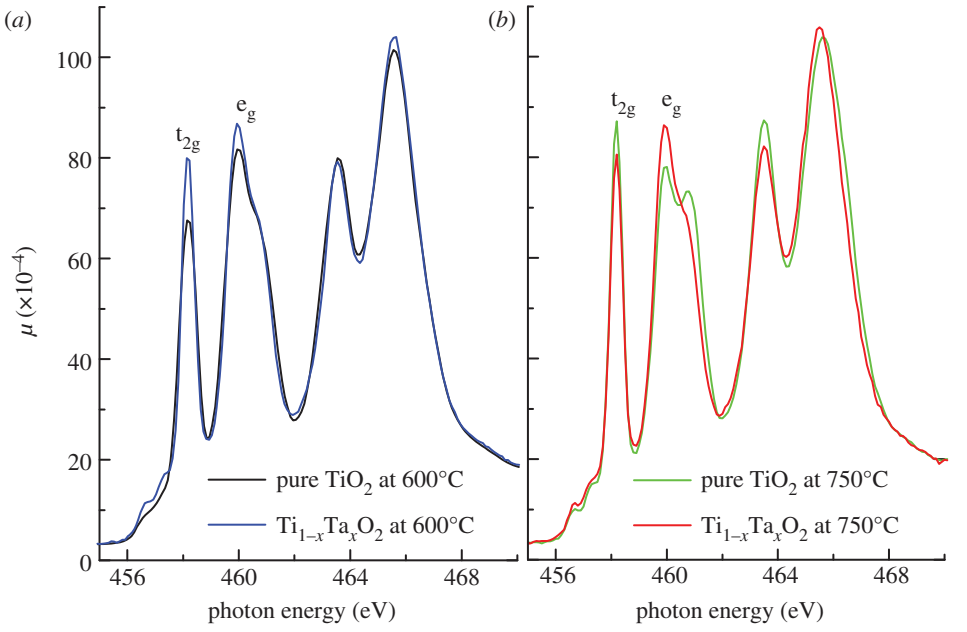

Figure 9. The XAS for pure TiO_2 and $Ti_{1-x}Ta_xO_2$ ($x \sim 0.05$) samples grown at (*a*) 600°C and (*b*) 750°C. The XAS for $Ti_{1-x}Ta_xO_2$ ($x \sim 0.05$) sample grown at 600°C shows anomalous enhancement of the spectral weight in t_{2g} states when compared with the pure TiO_2 grown at the same temperature, confirming the formation of a significant amount of V_{Ti} in $Ti_{1-x}Ta_xO_2$ films. By contrast, the XAS for $Ti_{1-x}Ta_xO_2$ ($x \sim 0.05$) sample grown at 750°C shows a decrease in the spectral weight in t_{2g} states when compared with the pure TiO_2 grown at 750°C, showing the absence of V_{Ti}. (Online version in colour.)

the spin-down (spin-up) unoccupied Ti 3d states. Interestingly, the calculated OMCD spectrum tracks very well with the experimental data, including the peak position and the width. This further supports that the FM truly arises from the intrinsic properties of the system.

(*d*) *Origin of ferromagnetism*

The evidence for FM from a variety of techniques is reassuring, and what is left is to figure out the nature of the cationic defect responsible for this. V_{Ti} and Ti^{3+} are the likely candidates, and we need spectroscopic evidence to identify their role. The XPS data in figure 3 show that the weakly ferromagnetic $Ti_{1-x}Ta_xO_2$ ($x \sim 0.05$) film grown at 750°C (best crystalline) exhibits 14 times higher Ti^{3+} signal than the ferromagnetic $Ti_{1-x}Ta_xO_2$ ($x \sim 0.05$) film grown at 600°C. These data rule out the role of Ti^{3+} in the FM seen.

The XAS spectra taken at the Ti $L_{2,3}$ edges from the pure TiO_2 and $Ti_{1-x}Ta_xO_2$ ($x \sim 0.05$) films (both grown at 600°C and 750°C) are shown after background correction [32–36] in figure 9*a*,*b*, respectively. The XAS signal of $Ti_{1-x}Ta_xO_2$ ($x \sim 0.05$) films grown at 600°C increases dramatically in the t_{2g} bands compared with the pure TiO_2 film grown at the same temperature. The

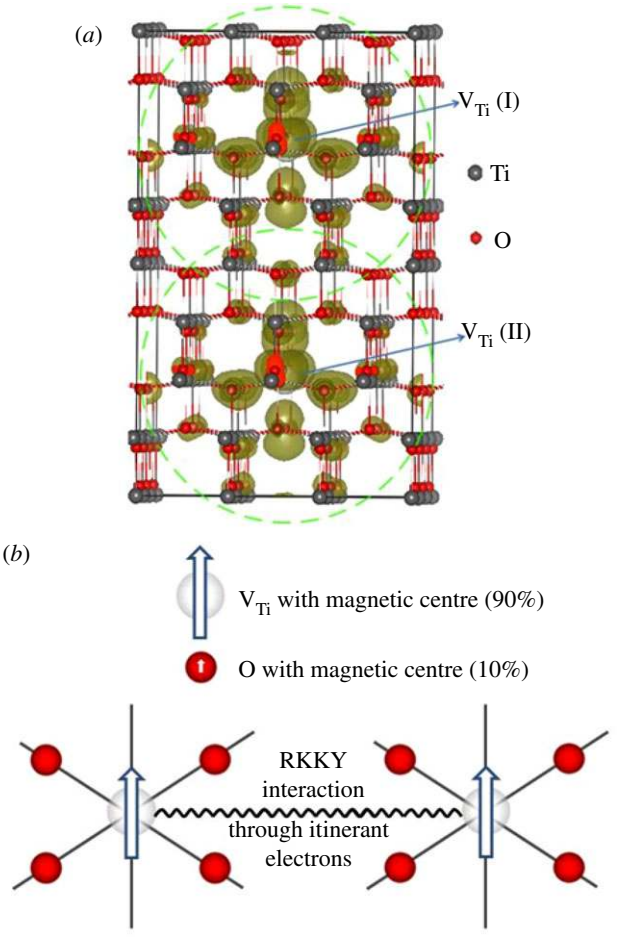

Figure 10. (*a*) Three-dimensional spin density plot of anatase TiO_2 with two V_{Ti}. The dark yellow isosurface represents the spin density of V_{Ti}, and dashed green circles show the range of the delocalized magnetic orbitals of V_{Ti}. (*b*) A schematic of the maximum possible ferromagnetic ordering of magnetic centres (grey circle) at the sites of Ti vacancies coupled by an itinerant-electron-mediated (RKKY) exchange mechanism. (Online version in colour.)

increasing spectral weight is direct evidence for the formation of V_{Ti} because a V_{Ti} creates four holes in the O 2p band, which is strongly hybridized with the Ti 3d band. The creation of these holes increases the number of unoccupied states near the Fermi level, e.g. in the t_{2g} bands, and therefore increases the XAS signal (which is also consistent with our theoretical calculations shown earlier). From the ratio of the t_{2g} to e_g bands for the pure TiO_2 and $Ti_{1-x}Ta_xO_2$ ($x \sim 0.05$) film grown at 600°C (figure 9*a*), we were able to estimate an upper limit of 3 per cent for V_{Ti}, with the actual number likely to be lower by a factor of 2 or more, as it did not account for all the defects that could increase the number of unoccupied states near the Fermi level. This number is a factor of 5 larger than the value one would obtain for the vacancy concentration based on charge compensation. Altogether, one can say for sure that the actual vacancy concentration is somewhere between

0.6 and 3 per cent. A much more detailed study would be needed to further narrow down these numbers. By the same analogy, when we compare the pure TiO_2 with $Ti_{1-x}Ta_xO_2$ ($x \sim 0.05$) films grown at 750°C (figure 9*b*), the t_{2g} peak of the latter decreases in height with respect to the former, which (together with the support of XPS data) suggests no or very reduced V_{Ti}.

In retrospect, it is important to note that the SXMCD signal in the present case is different from the one observed in $LaMnO_3/SrTiO_3$, which originates from the Ti^{3+} states present at its interface, as recently reported by Garcia-Barriocanal *et al.* [41]. This also suggests that the strong SXMCD signal in $Ti_{1-x}Ta_xO_2$ ($x \sim 0.05$) films grown at 600°C does not arise from the Ti^{3+} defect and is most likely from the V_{Ti}. All these facts also support the fact that the role of Ti^{3+}, if any, is secondary.

Now that V_{Ti} is established as the magnetic entity, we will try to develop a microscopic understanding of the FM. The four unpaired electrons in a Ti vacancy site can align in three possible ways, which will yield 4, 2 and 0 μ_B. Statistically, we can assume a value of 2 μ_B per vacancy, which would mean that, to get the magnetization value seen, an amount of approximately 2.5 per cent vacancy would be needed. In addition, to compensate 50 per cent of the free electrons from the Ta, about 0.6 per cent vacancies would be needed. So a total of about 3 per cent V_{Ti} is adequate to explain the saturation magnetization as well as the electron compensation seen, which is consistent with the predictions [22]. The average distance between two V_{Ti} is about 3–4 unit cells. Unless the orbital magnetization of the V_{Ti} is extended over at least two unit cells, the direct exchange probability is very low. The fact that is FM (but see Kondo scattering [23]) is not seen in samples prepared at higher oxygen pressures, where the V_{Ti} concentration is higher but the carrier concentration is lower, strongly argues in favour of a carrier-mediated exchange [8,42]. Figure 10 shows a schematic of the mechanism where the origin of FM is related to magnetic centres associated with the V_{Ti}. As the free electron carrier density of the $Ti_{1-x}Ta_xO_2$ ($x \sim 0.05$) film is about $7.6 \times 10^{20}\,cm^{-3}$, the mechanism of FM is most probably facilitated through itinerant electron-mediated RKKY.

In conclusion, the FM seen in $Ti_{1-x}Ta_xO_2$ ($x \sim 0.05$) thin films prepared at 600°C is verified by a battery of magnetic measurements, and the role of magnetic artefacts was eliminated by a variety of analytical techniques. With close to 100 per cent substitutionality of the Ta, the activation of only 50 per cent of the Ta implied the presence of compensating defects such as V_{Ti} and Ti^{3+}. Further spectroscopic evidence clearly showed the role of V_{Ti} and not Ti^{3+}, leading to a mechanism where magnetic V_{Ti} were helped by RKKY exchange with the free electrons. This is the first demonstration of magnetism arising from cationic vacancies, which may pave the way for other novel magnetic phenomena.

The authors thank G. A. Sawatzky, H. Yang, S. B. Ogale, K. Gopinadhan, C. K. Yong, W. Xiao, K. Singal, R. Minqin, T. Osipowicz and F. Watt for their experimental help and fruitful discussions related to this work. This work is supported by NRF-CRP grant 'Tailoring Oxide Electronics by Atomic Control' NRF2008NRF-CRP002–024, NUS YIA, NUS cross-faculty grant, MOE AcRF Tier-2 grant (MOE2010-T2-2-121), FRC, BMBF and DFG. K.Y. and Y.D. are grateful for the financial support of the National Basic Research Program of China (Program 973, grant No. 2007CB613302).

References

1 Wolf, S. A., Awschalom, D. D., Buhrman, R. A., Daughton, J. M., Von Molnár, S., Roukes, M. L., Chtchelkanova, A. Y. & Treger, D. M. 2011 Spintronics: a spin-based electronics vision for the future. *Science* **294**, 1488–1495. (doi:10.1126/science.1065389)

2 MacDonald, A. H., Schiffer, P. & Samarth, N. 2005 Ferromagnetic semiconductors: moving beyond (Ga,Mn)As. *Nat. Mater.* **4**, 195–202. (doi:10.1038/nmat1325)

3 Korbecka, A. & Majewski, J. A. 2009 On the origin of room-temperature ferromagnetism in wide-gap semiconductors. *Low Temp. Phys.* **35**, 53. (doi:10.1063/1.3064909)

4 Ohno, H. 1998 Making nonmagnetic semiconductors ferromagnetic. *Science* **281**, 951–956. (doi:10.1126/science.281.5379.951)

5 Žutić, I., Fabian, J. & Das Sarma, S. 2004 Spintronics: fundamentals and applications. *Rev. Mod. Phys.* **76**, 323–410. (doi:10.1103/RevModPhys.76.323)

6 Ohno, Y., Young, D. K., Beschoten, B., Matsukura, F., Ohno, H. & Awschalom, D. D. 1999 Electrical spin injection in a ferromagnetic semiconductor heterostructure. *Nature* **402**, 790–792. (doi:10.1038/45509)

7 Oiwa, A., Mitsumori, Y., Moriya, R., Słupinski, T. & Munekata, H. 2002 Effect of optical spin injection on ferromagnetically coupled Mn spins in the III–V magnetic alloy semiconductor (Ga,Mn)As. *Phys. Rev. Lett.* **88**, 137202. (doi:10.1103/PhysRevLett.88.137202)

8 Behan, A. J., Mokhtari, A., Blythe, H. J., Score, D., Xu, X.-H., Neal, J. R., Fox, A. M. & Gehring, G. A. 2008 Two magnetic regimes in doped ZnO corresponding to a dilute magnetic semiconductor and a dilute magnetic insulator. *Phys. Rev. Lett.* **100**, 047206. (doi:10.1103/PhysRevLett.100.047206)

9 Shinde, S. R. *et al.* 2003 Ferromagnetism in laser deposited anatase $Ti_{1-x}Co_xO_{2-\delta}$ films. *Phys. Rev. B* **67**, 115211. (doi:10.1103/PhysRevB.67.115211)

10 Kundaliya, D. C. *et al.* 2004 On the origin of high-temperature ferromagnetism in the low-temperature-processed Mn–Zn–O system. *Nat. Mater.* **3**, 709–714. (doi:10.1038/nmat1221)

11 Matsumoto, Y. *et al.* 2001 Room-temperature ferromagnetism in transparent transition metal-doped titanium dioxide. *Science* **291**, 854–856. (doi:10.1126/science.1056186)

12 Chambers, S. A. *et al.* 2006 Ferromagnetism in doped thin-film oxide and nitride semiconductors and dielectrics. *Surf. Sci. Rep.* **61**, 345–381. (doi:10.1016/j.surfrep.2006.05.001)

13 Pan, H. *et al.* 2007 Room-temperature ferromagnetism in carbon-doped ZnO. *Phys. Rev. Lett.* **99**, 127201. (doi:10.1103/PhysRevLett.99.127201)

14 Kaspar, T. C. *et al.* 2005 Negligible magnetism in excellent structural quality $Cr_xTi_{1-x}O_2$ anatase: contrast with high-T_C ferromagnetism in structurally defective $Cr_xTi_{1-x}O_2$. *Phys. Rev. Lett.* **95**, 217203. (doi:10.1103/PhysRevLett.95.217203)

15 Elfimov, I. S., Rusydi, A., Csiszar, S. I., Hu, Z., Hsieh, H. H., Lin, H.-J., Chen, C. T., Liang, R. & Sawatzky, G. A. 2007 Magnetizing oxides by substituting nitrogen for oxygen. *Phys. Rev. Lett.* **98**, 137202. (doi:10.1103/PhysRevLett.98.137202)

16 Ogale, S. B. 2010 Dilute doping, defects, and ferromagnetism in metal oxide systems. *Adv. Mater.* **22**, 3125–3155. (doi:10.1002/adma.200903891)

17 Ando, K. 2006 Seeking room-temperature ferromagnetic semiconductors. *Science* **312**, 1883–1885. (doi:10.1126/science.1125461)

18 Abraham, D. W., Frank, M. M. & Guha, S. 2005 Absence of magnetism in hafnium oxide films. *Appl. Phys. Lett.* **87**, 252502. (doi:10.1063/1.2146057)

19 Kobayashi, M. *et al.* 2005 Characterization of magnetic components in the diluted magnetic semiconductor $Zn_{1-x}Co_xO$ by X-ray magnetic circular dichroism. *Phys. Rev. B* **72**, 201201. (doi:10.1103/PhysRevB.72.201201)

20 Herng, T. S. *et al.* 2010 Room-temperature ferromagnetism of Cu-doped ZnO films probed by soft X-ray magnetic circular dichroism. *Phys. Rev. Lett.* **105**, 207201. (doi:10.1103/PhysRevLett.105.207201)

21 Elfimov, I. S., Yunoki, S. & Sawatzky, G. A. 2002 Possible path to a new class of ferromagnetic and half-metallic ferromagnetic materials. *Phys. Rev. Lett.* **89**, 216403. (doi:10.1103/PhysRevLett.89.216403)

22 Osorio-Guillén, J., Lany, S. & Zunger, A. 2008 Atomic control of conductivity versus ferromagnetism in wide-gap oxides via selective doping: V, Nb, Ta in anatase TiO_2. *Phys. Rev. Lett.* **100**, 036601. (doi:10.1103/PhysRevLett.100.036601)
23 Zhang, S. X. *et al.* 2009 Electronic manifestation of cation-vacancy-induced magnetic moments in a transparent oxide semiconductor: anatase Nb:TiO_2. *Adv. Mater.* **21**, 2282–2287. (doi:10.1002/adma.200803019)
24 He, Y., Dulub, O., Cheng, H., Selloni, A. & Diebold, U. 2009 Evidence for the predominance of subsurface defects on reduced anatase TiO_2(101) *Phys. Rev. Lett.* **102**, 106105. (doi:10.1103/PhysRevLett.102.106105)
25 Hashimoto, S., Tanaka, C., Murata, A. & Sakurada, T. 2006 Formulation for XPS spectral change of oxides by Ar ion bombardment: application of the formulation to Ta_2O_5 system. *J. Surf. Anal.* **13**, 14–18.
26 Roy Barman, A. *et al.* 2011 Multifunctional $Ti_{1-x}Ta_xO_2$: Ta doping or alloying? *Appl. Phys. Lett.* **98**, 072111. (doi:10.1063/1.3553773)
27 Yu, J. *et al.* 2005 New soft X-ray facility SINS for surface and nanoscale science at SSLS. *J. Electron Spectrosc. Relat. Phenom.* **144**, 1031–1034. (doi:10.1016/j.elspec.2005.01.256)
28 Thole, B., Carra, P., Sette, F. & van der Laan, G. 1992 X-ray circular dichroism as a probe of orbital magnetization. *Phys. Rev. Lett.* **68**, 1943–1946. (doi:10.1103/PhysRevLett.68.1943)
29 Carra, P., Thole, B., Altarelli, M. & Wang, X. 1993 X-ray circular dichroism and local magnetic fields. *Phys. Rev. Lett.* **70**, 694–697. (doi:10.1103/PhysRevLett.70.694)
30 J. Stöhr. 1999 Exploring the microscopic origin of magnetic anisotropies with X-ray magnetic circular dichroism (XMCD) spectroscopy. *J. Magn. Magn. Mater.* **200**, 470–497. (doi:10.1016/S0304-8853(99)00407-2)
31 Henke, B. L., Gullikso, E. M. & Davis, J. C. 1993 X-ray interactions: photoabsorption, scattering, transmission, and reflection at $E = 50$–$30{,}000\,\mathrm{eV}$, $Z = 1$–92. *At. Data Nucl. Data Tables* **54**, 181–342. (doi:10.1006/adnd.1993.1013)
32 Abbamonte, P., Venema, L., Rusydi, A., Sawatzky, G. A., Logvenov, G. & Bozovic, I. 2002 A structural probe of the doped holes in cuprate superconductors. *Science* **297**, 581–584. (doi:10.1126/science.1070903)
33 Abbamonte, P., Rusydi, A., Smadici, S., Gu, G. D., Sawatzky, G. A. & Feng, D. L. 2005 Spatially modulated 'mottness' in $La_{2-x}Ba_xCuO_4$. *Nat. Phys.* **1**, 155–158. (doi:10.1038/nphys178)
34 Rusydi, A. *et al.* 2008 Strain amplification of the $4k_F$ chain instability in $Sr_{14}Cu_{24}O_{41}$. *Phys. Rev. Lett.* **100**, 036403. (doi:10.1103/PhysRevLett.100.036403)
35 Rusydi, A. 2006 Resonant soft X-ray scattering and charge density waves in correlated systems. PhD dissertation, University of Groningen, The Netherlands.
36 de Groot, F. M. F., Grioni, M., Fuggle, J. C., Ghijsen, J., Sawatzky, G. A. & Petersen, H. 1989 Oxygen 1s X-ray-absorption edges of transition-metal oxides. *Phys. Rev. B* **40**, 5715–5723. (doi:10.1103/PhysRevB.40.5715)
37 de Groot, F. M. F., Faber, J., Michiels, J. J. M., Czyżyk, M. T., Abbate, M. & Fuggle, J. C. 1993 Oxygen 1s X-ray absorption of tetravalent titanium oxides: a comparison with single-particle calculations. *Phys. Rev. B* **48**, 2074–2080. (doi:10.1103/PhysRevB.48.2074)
38 Rauer, R., Neuber, G., Kunze, J., Bäckström, J. & Rübhausen, M. 2005 Temperature-dependent spectral generalized magneto-optical ellipsometry for ferromagnetic compounds. *Rev. Sci. Instr.* **76**, 023910. (doi:10.1063/1.1834702)
39 Rauer, R., Rübhausen, M. & Dörr, K. 2006 Magnetic-order induced spectral-weight redistribution in $La_{0.7}(Sr,Ca)_{0.3}MnO_3$. *Phys. Rev. B* **73**, 092402. (doi:10.1103/PhysRevB.73.092402)
40 Hay, P. J., Thibeault, J. C. & Hoffmann, R. 1995 Orbital interactions in metal dimer complexes. *J. Am. Chem. Soc.* **97**, 4884–4899. (doi:10.1021/ja00850a018)
41 Garcia-Barriocanal, J. *et al.* 2010 Spin and orbital Ti magnetism at $LaMnO_3/SrTiO_3$ interfaces. *Nat. Commun.* **1**, 82. (doi:10.1038/ncomms1080)
42 Wessels, B. W. 2008 Ferromagnetic semiconductors and the role of disorder. *New J. Phys.* **10**, 055008. (doi:10.1088/1367-2630/10/5/055008)